PERGAMON

Journal of South American Earth Sciences 14 (2002) 837–849

Journal of
South American
Earth Sciences

www.elsevier.com/locate/jsames

Geology and geochemistry of the Caxias gold deposit, and geochronology of the gold-hosting Caxias Microtonalite, São Luís Craton, northern Brazil

E.L. Klein[a,*], J.C. Koppe[b], C.A.V. Moura[c]

[a]*CPRM/Geological Survey of Brazil, Av. Dr Freitas, 3645, Belém, PA 66095-110, Brazil*
[b]*Universidade Federal do Rio Grande do Sul, Av. Oswaldo Aranha, 99/504, Porto Alegre, RS 90035-190, Brazil*
[c]*Centro de Geociências, Universidade Federal do Pará, Caixa Postal 1611, Belém, PA 66000-000, Brazil*

Received 1 March 2001; accepted 1 August 2001

Abstract

The Caxias gold deposit, located in the São Luís Craton, is hosted by a steeply dipping strike-slip shear zone crosscutting schists and a fine-grained, hydrothermally altered tonalite (Caxias Microtonalite). Petrography and whole-rock geochemistry have characterized both pelitic and mafic protoliths for the hosting schists. The Caxias Microtonalite shows major and trace element behavior compatible with modern calc-alkaline, metaluminous, subduction-related granitoids. Geochronological studies on the Caxias Microtonalite have defined a minimum crystallization age of 1985 ± 4 Ma, obtained by single-zircon Pb evaporation, and Sm–Nd crustal residence age (T_{DM}) of 2.17 Ga, with $\varepsilon Nd(T)$ +0.74, suggesting a juvenile protolith. The exact origin and role of the Caxias Microtonalite remain uncertain. It may be interpreted as representing either a late manifestation of the regionally dominant Tromaí magmatism, or a juvenile episode unrelated to this major magmatism. Rock, quartz veins, and saprolite geochemistry have shown that As, Sb, Ba, Rb, V, Cr, Co, and Ni, as well as Au, are useful elements that can be used in exploration for similar deposits in the region.

Keywords: Gold; Paleoproterozoic; Geochronology; Geochemistry; Shear zone

1. Introduction

The Gurupi Auriferous Province of northern Brazil, comprising the São Luís Craton and the Gurupi Belt (Fig. 1), has been a minor gold producer since the second half of the seventeenth century. The decreasing of the alluvial and supergene gold production has led to the discovery of small primary deposits and showings (e.g. Caxias, Areal, Pedra de Fogo, Novo Destino, Mina Seca), which have been exploited by small prospectors (*garimpeiros*), drawing the attention of mining companies. Several deposits have been intensively drilled (e.g. Cachoeira, Montes Áureos, Serrinha), and a few have estimated resources around 18 tons (Aurizona), and 66 tons of gold (Chega Tudo).

This region has also been the subject of a recent regional mapping program performed by the Geological Survey of Brazil (Pastana, 1995; Costa, 2000; Almeida, 2000), which redefined the regional lithostratigraphy, previously established mainly by Costa et al. (1977) and Abreu et al. (1980). However, the chronology of the magmatic, metamorphic, and deformational events is still poorly constrained, and based only on Rb–Sr and K–Ar isotopic systems. The knowledge of the gold metallogeny of the Gurupi Province is also scarce, lacking geological and analytical data on a regional scale. Nevertheless, some research has been done, especially on fluid inclusions, in order to place some constraints on the genesis of individual deposits, such as Montes Áureos (Yamaguti and Villas, 1999), Pedra de Fogo (Klein et al., 2000a), and Caxias and Areal (Klein, 1998; Klein et al., 2000b).

As a contribution to the stepwise enhancement of the understanding of the regional geology and gold metallogeny of the São Luís Craton, this paper presents the geological characterization of the Caxias deposit (unofficial production of more than 1 ton of gold). Special attention is given to the mineralized Caxias Microtonalite, a newly described lithodemic unit. Interpretations are based on fieldwork, rock geochemistry, and Pb–Pb and Sm–Nd geochronology. Some comments on the importance of this study for regional exploration are included as well.

2. Geological setting

Three major geotectonic units are recognized in the Gurupi region, northern Brazil (Fig. 1): the São Luís Craton,

* Corresponding author. Tel.: +55-21-91-276-8577; fax: +55-21-91-276-4020.
E-mail address: eklein@amazon.com.br (E.L. Klein).

0895-9811/02/$ - see front matter
PII: S0895-9811(01)00075-X

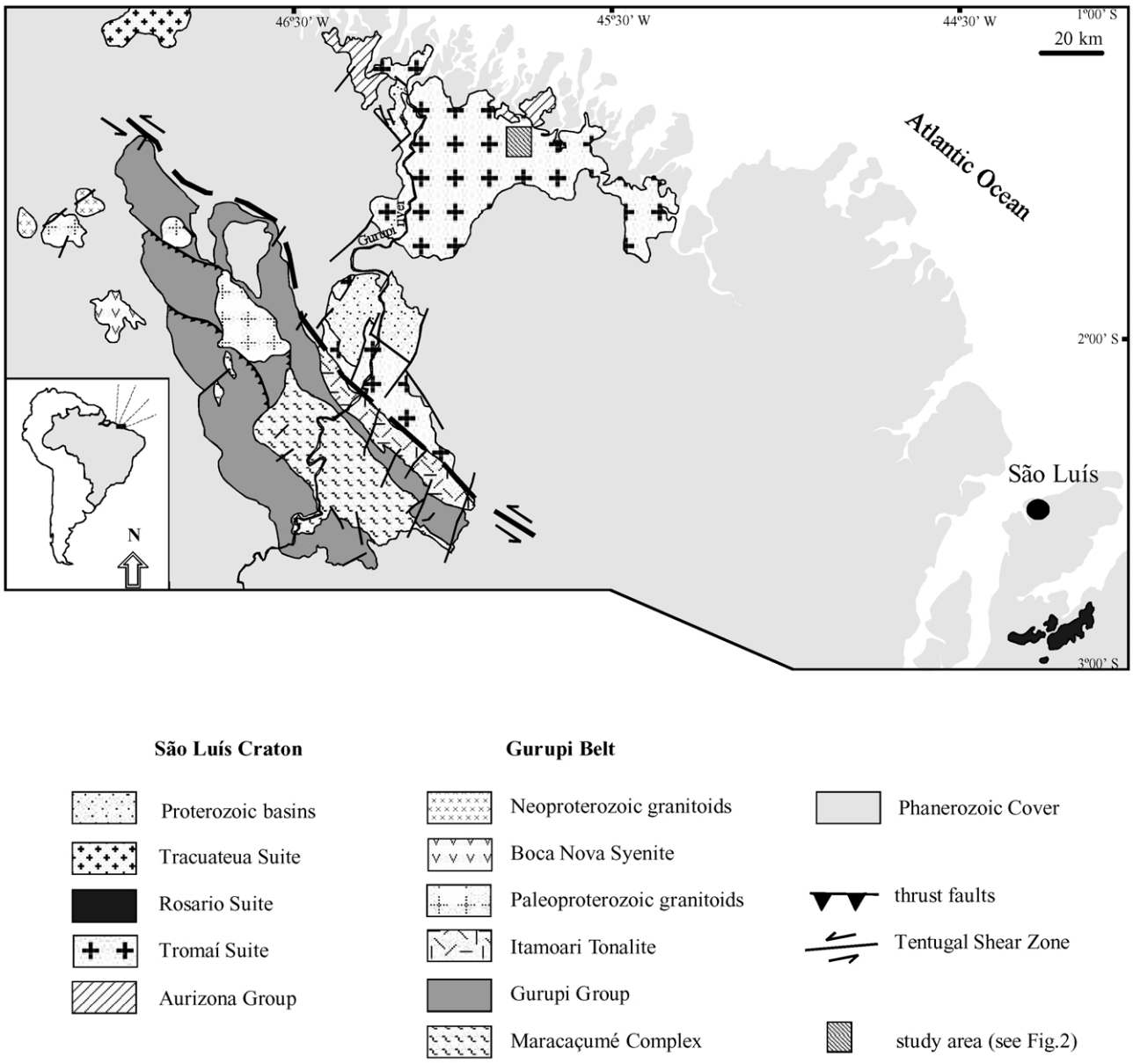

Fig. 1. Location map (inset) and regional geological map of the Gurupi and São Luís/Rosário regions, in northern Brazil. Compiled from Rodrigues et al. (1994), Pastana (1995), Costa (2000), and Almeida (2000).

the Gurupi Belt, and sedimentary basins. The São Luís Craton has been considered a fragment of the West African Craton from which it was separated during the breakup of the Pangea supercontinent in the Phanerozoic (Bullard et al., 1965; Hurley et al., 1967; Lesquer et al., 1984; Ledru et al., 1994). Its geological evolution is essentially linked to the Paleoproterozoic, especially around 2.1 Ga, as attested by K–Ar, Rb–Sr (Hurley et al., 1967; Almeida et al., 1968; Cordani et al., 1968; Almaraz and Cordani, 1969) and scarce Sm–Nd model ages and Pb–Pb zircon dating (Souza, 1995; Gaudette et al., 1996; Sato, 1998; Gorayeb et al., 1999).

The São Luís Craton is composed dominantly of granitoids and of minor metavolcano-sedimentary rocks. The Tromaí Suite (Pastana, 1995) is the predominant lithostratigraphic unit and encompasses multiphase granitoid batholiths. This suite is further subdivided into the Cândido Mendes Tonalite, composed of tonalites, granodiorites, and trondhjemites, and the subordinate Areal Granite (syenogranites and monzogranites). Both have chemical characteristics comparable with those of calc-alkaline, metaluminous to peraluminous granitoids, analogous to TTG and to modern subduction-related volcanic arc granitoids (Pastana, 1995; Klein, 1998). The Tromaí granitoids underwent localized greenschist metamorphism and they are largely unaffected by tectonic deformation, maintaining their primary igneous characteristics. This is due to the fact that, structurally, the craton is largely undeformed, hosting only discrete, centimeter- to meter-wide shear zones, which

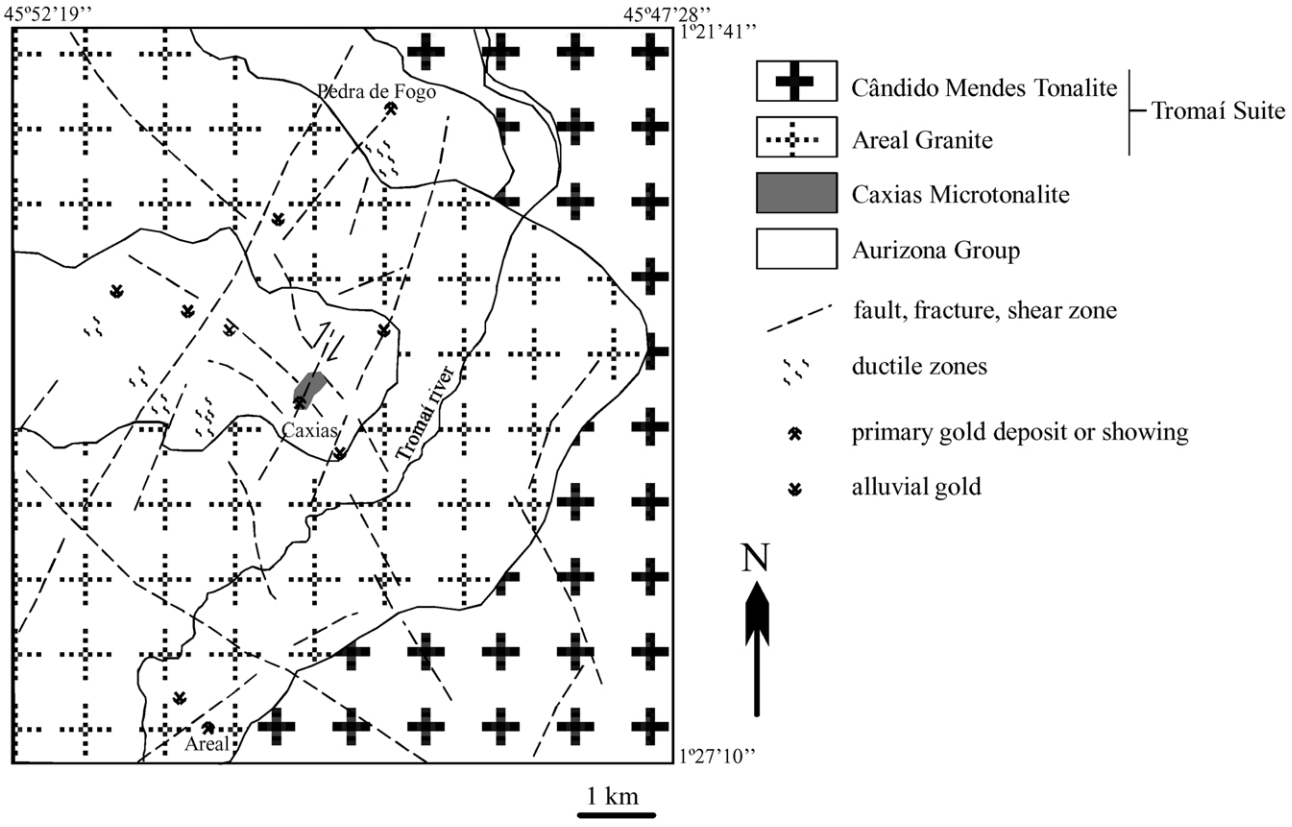

Fig. 2. Geological map of the Caxias deposit region.

are, nonetheless, gold-hosting structures. These features are different from the Gurupi Belt, which is strongly lineated and sheared. Subordinate dacites and rhyodacites have also been described as being associated with the Tromaí magmatism (Pastana, 1995). Other granitoids, which have been correlated to the Tromaí Suite, are those from Rosário (Rodrigues et al., 1994; Gorayeb et al., 1999) and Tracuateua (Costa, 2000) Suites (Fig. 1).

The metavolcano-sedimentary rocks of the Aurizona Group, composed of schists of variable compositions, phyllite, metachert, and metamafic to metaultramafic rocks, were grouped by Pastana (1995). The metasedimentary rocks dominate over the metavolcanics and both were metamorphosed under greenschist conditions (locally attaining lower amphibolite facies).

The Tromaí and Aurizona cratonic sequences have been proposed as belonging to a greenstone–granite terrain (Abreu, 1990; Pastana, 1995), but Costa and Ricci (1995) have argued against this hypothesis, suggesting that the subordinate occurrence of metaigneous rocks relative to metasedimentary rocks, the virtual absence of iron formations and the irregular (not linear) distribution of the supracrustal sequences are not consistent with typical greenstone belts. Nevertheless, considering the correlation between the São Luís and West African Cratons, the Birimian sequences of the latter have been regarded as examples of Proterozoic greenstone belts by Condie (1982) and Smith (1992). In addition, the dominance of metasedimentary rocks over the metaigneous is a common feature of Paleoproterozoic greenstone belts (Goodwin, 1996).

The São Luís Craton is bounded to the SSW by the Gurupi Belt (Fig. 1), whose age, longitudinal and lateral extension, lithostratigraphy, structural domains, and geological evolution are still under debate (Abreu, 1990; Costa and Ricci, 1995; Pastana, 1995; Gorayeb et al., 1999). Regardless of what the interpretations are, this belt is composed by strongly deformed and subparallel metasedimentary and metavolcanic rocks, which alternate with gneisses and irregularly deformed granitoids (Pastana, 1995; Costa, 2000; Almeida, 2000).

Proterozoic basins and Phanerozoic sedimentary cover (Fig. 1) hinder a better assessment of the older geology.

3. Local geology and deposit description

In the region of the Caxias gold deposit, granitoids of the Tromaí Suite (Cândido Mendes Tonalite and Areal Granite), along with schists, metavolcanic, and metapyroclastic rocks from the Aurizona Group, and the mineralized Caxias Microtonalite crop out (Fig. 2). The Tromaí granitoids are dominantly monzogranitic in composition and exhibit equigranular to porphyritic textures. They are largely undeformed, except in centimeter- to meter-wide shear zones,

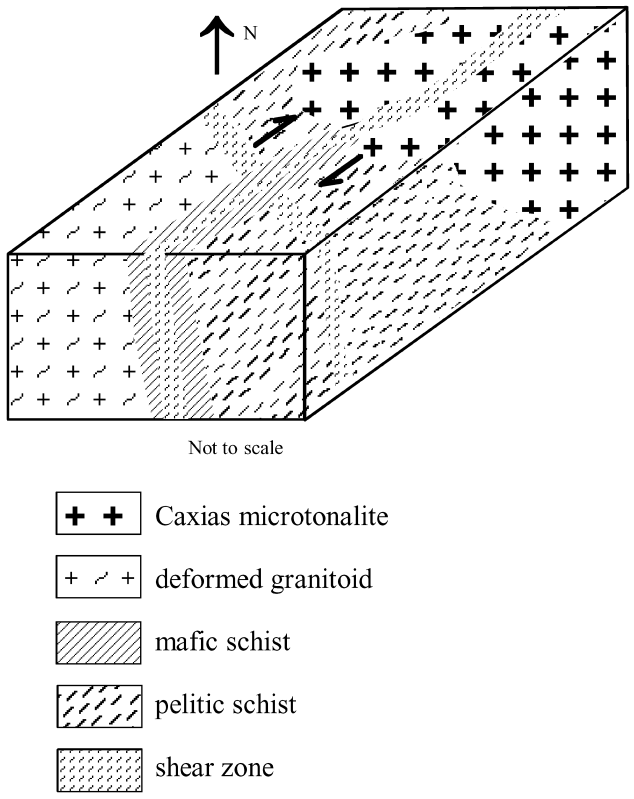

Fig. 3. Schematic block diagram showing the geology of the Caxias gold deposit (not to scale).

some of which host gold-bearing quartz veins, as in the Areal mineralization. Schists and foliated pyroclastic rocks (volcanic agglomerates, tuffs), which also host gold deposits, crop out at the central and northern portion of the area near the Pedra de Fogo township (Fig. 2).

Gold mineralization at Caxias is associated with a 0.2–1.0-m-thick, ductile–brittle shear zone, striking to N15°E; 75°SE, containing abundant, continuous to discontinuous quartz veinlets. This shear zone crosscuts both the schists and the Caxias Microtonalite (Fig. 3) and is surrounded by a meter-wide hydrothermal halo, which is also mineralized.

The Caxias Microtonalite was first referred by Leão Neto (1993) as a fine-grained rock affected by pervasive hydrothermal alteration, crosscut by the NE-striking shear zone. In its least altered portions it is greenish-gray in color, having a massive equigranular texture. Where strongly altered, it is olive green, showing a subtle reorientation of the mafic minerals, disseminations of pyrite and veinlets of quartz and late-stage carbonate. The actual extent of the microtonalite body is unknown, but field evidence indicates a small, shallow intrusion in the schists, a few hundred meters in length and tens of meters in width.

The schists are characterized by a strong subvertical foliation that parallels the strike of the shear zone. In addition to the vertical foliation, other structural elements observed within the schists are stretching lineations, and deformed quartz and quartzo–feldspathic veins. The stretching lineations are observed in quartz and phyllosilicates, both plunging 30–60° to NE. Few quartzo–feldspathic veins are boudinaged and some occur as rootless, intrafolial folds, which have been regarded as product of intense deformation, which started with a period of compression, and hence folding was followed by strong extension (cf. Ramsey and Huber, 1987; Park, 1989). The asymmetry of the intrafolial folds and the position of the stretching lineations indicate a dextral movement with an oblique component to the shear zone. Another meter-wide NW-trending shear zone also occurs at Caxias, but no crosscutting relationships were observed in the field between the two (NW and NE) structures.

In addition to the folded and boudinaged veins, quartz veins and veinlets fill fractures that crosscut the schists and the microtonalite in the mineralized zone. Although multidirectional, veinlets striking N25–35°E (subparallel to the schistosity) and N25–50°W are predominant. To the southwest, the schists are in contact with a deformed porphyritic granitoid, possibly a phase of the Areal Granite, and envelope meter-sized pockets of a sacharoidal to aplitic granitoid. The schists contain also centimeter- to decimeter-wide enclaves or small lenses of both deformed and preserved mafic rocks (amphibolite and gabbro/diorite, respectively). The deformed (foliated) small lenses are stretched in the direction of the schists' foliation.

Fluid inclusion studies of the quartz veinlets (Klein et al., 2000b) defined the mineralizing fluid as a reduced, low-salinity (<5 wt% NaCl equiv.), aqueous-carbonic fluid, containing 6–45 mol% CO_2 and up to 2.5 mol% N_2. Within the schists, this fluid has been enriched in CH_4 and, especially, N_2. This fact was interpreted as related to the reaction of the mineralizing fluid with carbonaceous matter present in the Aurizona schists (Klein, 1998). Fluid inclusion data combined with chlorite geothermometry (Klein and Koppe, 2000) bracket the *T–P* conditions to 262–307 °C and 1.6–4.6 kb, which places the deposit within the mesozonal to epizonal categories, according to the study of Gebre-Mariam et al. (1995).

3.1. Petrography and wall-rock alteration

In thin sections, the least-altered microtonalite consists of limpid and anhedral quartz crystals having variable but up to moderate undulose extinction. Plagioclase is the dominant mineral phase, occurring as elongated prisms with curved twins, covered by fine crystals of hydrothermal white mica growing along the crystalographic planes of the plagioclase. K-feldspar occurs only locally, showing an alteration pattern similar to that of plagioclase. Biotites are volumetrically important, occurring as elongated and randomly orientated platy grains, with pleochroism varying between pale brown, when fresh, and green, when altered to chlorite. Epidote is abundant, occurring in association with biotite and white mica; zircon and apatite occur as trace minerals, and cubic pyrite compose up to 2 vol% of the rock.

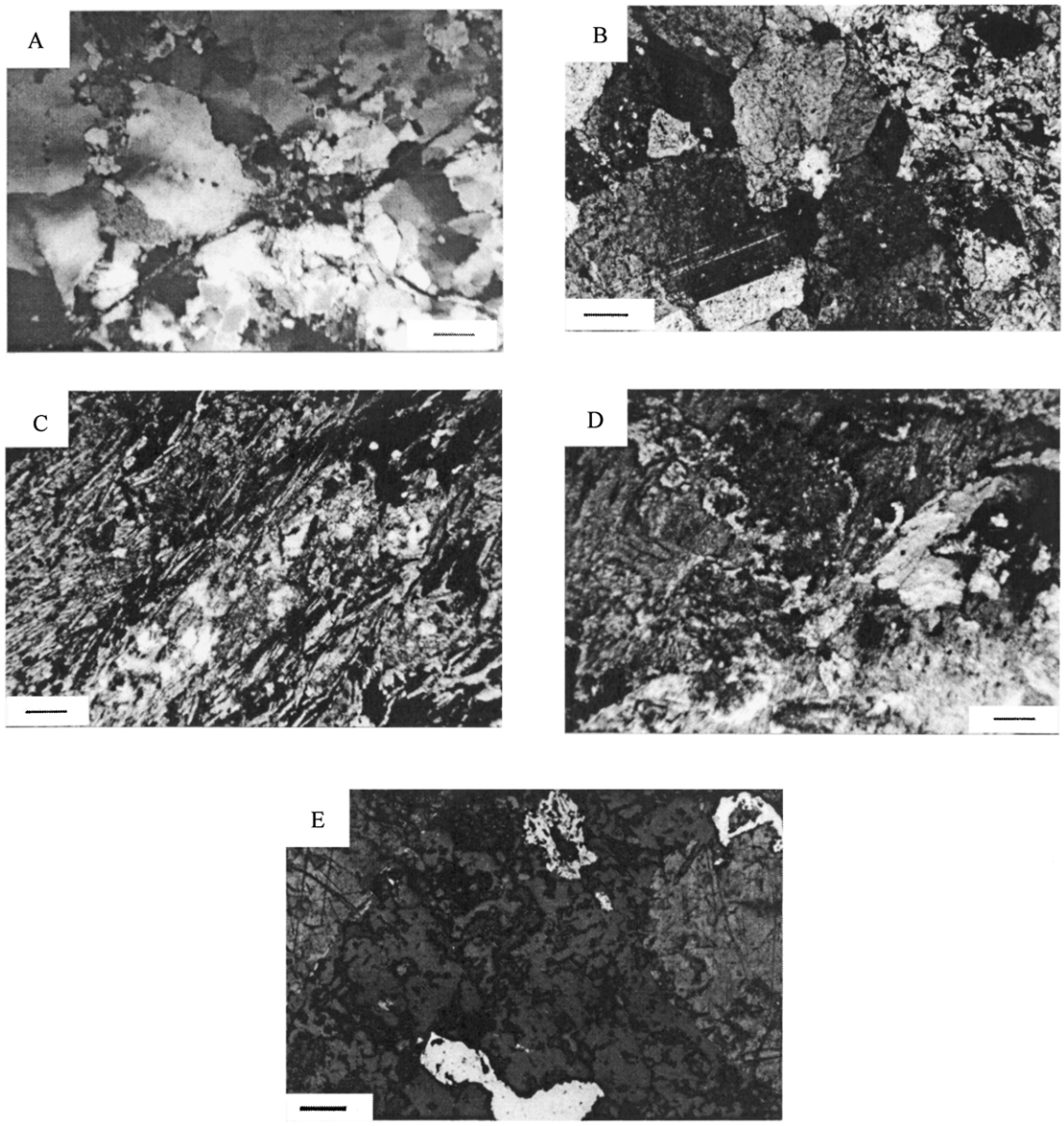

Fig. 4. Photomicrographs of rocks from the Caxias gold deposit. (a) Late carbonate veinlet crosscutting vein quartz and hydrothermal matrix of quartz, chlorite, and white mica in the Caxias Microtonalite (scale bar is 0.4 mm). (b) Local preservation of the plagioclase (left) close to a mass of white mica and quartz (right) in the Caxias Microtonalite (scale bar is 0.2 mm). (c) Mafic schist with lepidoblastic texture showing dissemination of sulphides (black) and secondary agglomerates of epidote (white) (scale bar is 0.4 mm). (d) Gabbro lens with chloritized hornblende (dark) along with altered plagioclase (scale bar is 0.4 mm). (e) Pyrite (bottom) and pyrite–sphalerite intergrowth (top), both enveloped by silicate gangue composed by quartz–chlorite–carbonate, occurring in the wall-rock alteration of the mineralized Caxias Microtonalite (scale bar is 0.2 mm).

When strongly hydrothermally altered, the microtonalite is finer grained than its less-altered portions and the primary igneous mineralogy is almost entirely pseudomorphosed. Only relics of plagioclase occur after the substitution by carbonate, white mica, and epidote, while the K-feldspar is no longer recognizable. Chlorite has substituted for all the biotite and occurs as fine, broadly oriented, and elongated crystals, with pleochroism ranging from colorless to olive green. Frequently, chlorite occurs in association with pyrite, showing intergrowth textures. Fine-grained quartz is distributed along with a matrix of carbonate, chlorite, white mica, and pyrite (Fig. 4(a) and (b)), showing a weak orientation. Outside the zone of strain concentration of the shear zone, the microtonalite shows a slight orientation of the mafic minerals, and quartz displays undulose extinction, minor subgrain development, and rare recrystallization.

Two different petrographic types of schists are found in Caxias. The first one hosts gold dissemination and is composed by similar proportions of biotite and chlorite of primarily uniform grain size. Both minerals are elongated and strongly oriented, defining the schistosity of the rock (Fig. 4(c)). White mica is subordinate, occurring either

Table 1
Whole-rock chemical composition of rocks from the Caxias gold deposit. CMT: Caxias Microtonalite; major elements in wt%; trace elements in ppm, except gold (ppb)

	Least altered, CMT	Hydroterm., CMT	Mafic schists		Mafic enclave	Pelitic schists	
	CX 47	CX 65	CX 64	CX 18	CX 43B	CX 04B	CX 10B
SiO_2	63.96	60.66	27.43	45.33	42.32	44.10	47.97
TiO_2	0.89	0.78	4.88	0.52	2.40	1.81	2.72
Al_2O_3	15.43	15.10	14.58	19.61	15.46	16.19	11.26
$Fe_2O_3^*$	7.39	7.33	27.21	12.08	18.85	18.92	19.27
MnO	0.17	0.12	0.20	0.10	0.17	0.12	0.22
MgO	1.41	1.07	5.81	4.66	7.33	2.94	3.76
CaO	4.09	4.29	4.99	2.66	13.02	6.41	0.96
Na_2O	4.86	4.93	0.10	1.70	0.10	< 0.10	< 0.10
K_2O	1.62	1.15	0.48	2.61	< 0.10	0.20	0.39
P_2O_5	0.31	0.27	0.10	0.10	0.08	0.19	0.26
LOI	1.70	4.73	13.28	11.21	2.12	7.20	8.88
Total	100.83	100.43	99.06	100.58	101.85	101.05	99.97
Ba	600.0	670.0	175.0	1781.0	650.0	310.0	< 50.0
Rb	26.0	< 15.0	31.0	82.0	1.0	14.0	28.0
Sr	379.0	361.0	308.0	340.0	309.0	386.0	73.0
Cs	< 1.0	4.0	3.0	4.0	< 1.0	2.0	< 1.0
Zr	111.0	123.0	12.0	3.0	31.0	47.0	22.0
Y	32.0	32.0	4.0	10.0	–	–	–
Th	3.1	3.6	< 0.2	< 0.2	< 0.2	1.0	< 0.2
U	1.4	< 0.5	< 0.5	< 0.5	< 0.5	< 0.5	1.7
Hf	4.0	5.0	< 1.0	1.0	< 1.0	1.0	< 1.0
Cr	17.0	25.0	40.0	690.0	26.0	20.0	20.0
Ni	< 15.0	< 15.0	20.0	530.0	< 20.0	< 20.0	20.0
Co	6.0	7.0	78.0	68.0	28.0	19.0	47.0
Sc	16.0	17.0	36.0	29.0	29.0	29.0	84.0
V	12.0	17.0	1319.0	167.0	–	–	–
Cu	1.0	81.0	10.0	1.0	83.0	115.0	62.0
Pb	1.0	3.0	7.0	4.0	1.0	5.0	2.0
Zn	228.0	84.0	260.0	170.0	179.0	140.0	410.0
Mo	< 1.0	< 1.0	< 1.0	< 1.0	< 1.0	< 1.0	3.0
W	< 1.0	< 1.0	240.0	< 1.0	23.0	< 1.0	30.0
As	4.6	3.0	1.9	120.0	3.8	4.5	6.3
Sb	1.1	0.5	0.3	0.2	0.6	0.3	< 0.1
Au	13.0	73.0	300.0	590.0	189.0	3000.0	290.0
La	34.00	30.00	1.90	8.60	3.30	7.70	4.90
Ce	71.00	64.00	< 3.00	14.00	6.00	9.00	9.00
Nd	35.00	30.00	< 5.00	11.00	< 5.00	< 5.00	< 5.00
Sm	7.50	6.70	0.60	2.20	1.00	1.30	1.50
Eu	2.20	1.90	0.90	1.10	0.80	0.60	0.90
Tb	0.80	< 0.50	< 0.50	< 0.50	< 0.50	< 0.50	< 0.50
Yb	3.90	3.20	0.80	1.10	–	1.00	1.90
Lu	0.67	0.47	0.13	0.14	0.13	0.14	0.28

concordant or discordantly with the foliation, often associated with clusters of epidote. Opaque minerals are voluminous (up to 15 vol%) and disseminated throughout the rock, while quartz occurs only as microveinlets both concordant and discordant with the foliation. The other petrographic type of schist is quartz rich. This mineral is fine grained, limpid, and virtually devoid of undulose extinction, suggesting the static recrystallization of the grains. White micas are abundant, occurring as a groundmass of fine-grained platy grains, as well as larger crystals. Relics of prismatic minerals, possibly altered feldspars, are found locally.

Decimeter-wide mafic fragments, petrographically characterized as foliated amphibolites and massive metamorphosed gabbro/diorite, were found as enclaves in the biotite–chlorite schists. Both are composed of hornblende/actinolite, chlorite, and intensively altered plagioclase with subordinate carbonate and opaque minerals (Fig. 4(d)).

Sulphides are widespread in the microtonalite. Reflected light microscopy has revealed pyrite as the dominant phase, occurring as subhedral to anhedral limpid crystals, either isolated or intergrown with chlorites and/or sphalerite (Fig. 4(e)). Sphalerite is anhedral and is distributed in the same manner as pyrite, but in lesser amounts. In the schists,

Table 2
Chemical composition of trace elements (ppm) and gold (ppb) from quartz veins and veinlets in the Caxias gold deposit

Sample	04a	10a	22	42a	42b	42c	42e	48	61d	62c	32a
Ba	300.0	220.0	260.0	110.0	100.0	370.0	150.0	130.0	170.0	150.0	260.0
Rb	< 1.0	< 1.0	2.0	< 1.0	< 1.0	47.0	1.0	< 1.0	< 1.0	1.0	2.0
Sr	< 1.0	9.0	13.0	19.0	18.0	305.0	302.0	2.0	9.0	12.0	13.0
Cs	< 1.0	< 1.0	< 1.0	< 1.0	< 1.0	5.0	< 1.0	< 1.0	< 1.0	< 1.0	< 1.0
Zr	127.0	< 2.0	< 2.0	2.0	< 2.0	61.0	56.0	< 2.0	< 2.0	3.0	< 2.0
Th	23.0	< 0.2	< 0.2	0.5	0.4	0.9	1.2	< 0.2	0.5	0.6	0.5
U	12.0	< 0.5	< 0.5	< 0.5	0.7	< 0.5	1.9	< 0.5	< 0.5	0.7	0.7
Hf	10.0	< 1.0	< 1.0	< 1.0	< 1.0	2.0	1.0	< 1.0	< 1.0	< 1.0	< 1.0
Cr	22.0	42.0	26.0	28.0	38.0	52.0	48.0	34.0	33.0	36.0	43.0
Ni	< 20.0	54.0	< 20.0	< 20.0	< 20.0	< 20.0	< 20.0	< 20.0	< 20.0	< 20.0	< 20.0
Co	8.0	27.0	21.0	4.0	2.0	28.0	18.0	2.0	14.0	2.0	20.0
Sc	1.6	0.5	2.4	1.9	1.4	35.0	18.0	0.5	0.9	1.4	2.4
Cu	14.0	22.0	31.0	25.0	12.0	0.5	38.0	8.0	10.0	9.0	29.0
Pb	7.0	2.0	2.0	1.0	4.0	47.0	6.0	3.0	< 0.5	0.5	3.0
Zn	4.0	16.0	53.0	10.0	8.0	243.0	159.0	2.0	7.0	60.0	19.0
Mo	12.0	4.0	6.0	< 1.0	5.0	< 1.0	< 1.0	< 1.0	< 1.0	3.0	< 1.0
W	4.0	6.0	27.0	5.0	< 1	21.0	110.0	2.0	4.0	7.0	< 1.0
As	3.0	4.0	9.6	2.8	4.6	15.0	10.0	2.0	2.1	2.6	12.0
Sb	0.4	0.3	2.7	2.7	2.2	0.7	3.0	2.1	2.1	2.4	0.5
Au	1030	361	126	31	8	69	56	8	14	15	301
La	35.00	< 1.00	3.60	6.50	5.00	13.00	9.50	< 1.00	4.80	< 1.00	4.30
Ce	71.00	< 3.00	< 3.00	11.00	6.00	25.00	19.00	< 3.00	8.00	< 3.00	8.00
Nd	28.00	< 5.00	< 5.00	7.00	< 5.00	12.00	7.00	< 5.00	< 5.00	< 5.00	< 5.00
Sm	6.30	< 0.10	0.60	1.00	0.80	3.50	2.60	< 0.10	0.60	< 0.10	1.10
Eu	0.50	< 0.20	0.30	0.30	0.20	2.70	2.10	< 0.20	< 0.20	< 0.20	0.40
Tb	< 0.50	< 0.50	< 0.50	< 0.50	< 0.50	0.70	< 0.50	< 0.50	< 0.50	< 0.50	< 0.50
Yb	3.30	< 0.20	0.30	0.40	0.30	2.40	2.00	< 0.20	0.20	< 0.20	0.60
Lu	0.54	< 0.05	< 0.05	< 0.05	< 0.05	0.36	0.33	< 0.05	0.05	< 0.05	0.08

sulphides occur also as disseminated grains. Pyrite is the dominant phase, with the presence of magnetite, sometimes growing after the pyrite. The quartz veinlets are sulphide-poor, containing basically anhedral pyrite associated with silicates (mainly chlorites) deposited in the quartz fractures.

A few free-gold particles were recognized, in both microtonalite and schists, occurring in the contact of quartz and chlorite grains, and spatially associated with the sulphides, while free-gold particles have not been petrographically recognized in the veinlets.

A latter generation of quartz occurs as veinlets (Fig. 4(a)), in which quartz is anhedral, coarse-grained, fractured, and showing undulose extinction and subgrain development. It is cut by microveinlets of both pyrite-bearing and pyrite-free carbonate. Small grains of apatite and epidote are dispersed along the rock. Deformation in these veins is essentially brittle, suggesting that their emplacement occurred late in the deformational history of the Caxias deposit. However, features like undulose extinction, subgrain development and deformation lamellae are also present, indicating that the quartz veinlets were also locally plastically deformed. These veinlets contain several populations of fluid inclusions, including primary carbonic and aqueous-carbonic inclusions, which were interpreted as the mineralizing fluid (Klein, 1998; Klein et al., 2000b). This indicates that the gold mineralizing event was late, but still associated with deformation in the Caxias shear zone.

4. Geochemistry

4.1. Sampling and analytical methods

Whole-rock chemical analyses of the microtonalite, schists, and quartz veins, as well as studies of the mineralizing fluids, were done in order to help the understanding of the geologic conditions under which the rocks at Caxias evolved. These data were assessed to see if a characteristic geochemical pattern might also be useful as an exploratory tool. The analyses were partially performed at the Universidade Federal do Rio Grande do Sul, by X-ray fluorescence and atomic absorption, and partially at the Activation Laboratories Ltd., by ICP-MS and INAA.

4.2. Results and discussion

The results are presented in Tables 1–3, and show that the hydrothermally altered microtonalite is K_2O enriched (comparison made on water- and volatile-free basis, best shown in Fig. 5(a)), with MgO, MnO, and SiO_2 slightly depleted in relation to the least altered sample. The high-iron content is probably related to the strong chloritization and sulphidation. The rest of the major elements show little modification in their contents, probably due to an internal chemical rearrangement related to the mineralogical changes that occurred during the hydrothermal event. The

Table 3
Trace element (ppm) and gold (ppb) chemical composition of saprolites from schists and from the Caxias Microtonalite (CMT) in the Caxias gold deposit

Sample	Schists				CMT
	11a	15a	17b	23b	46
Ba	< 50.0	1400.0	360.0	230.0	1300.0
Rb	45.0	88.0	16.0	12.0	127.0
Sr	285.0	456.0	402.0	508.0	12.0
Cs	3.0	3.0	5.0	2.0	2.0
Zr	154.0	56.0	45.0	56.0	335.0
Th	3.0	0.8	< 0.2	< 0.2	2.8
U	< 0.5	< 0.5	< 0.5	< 0.5	< 0.5
Hf	3.0	< 1.0	< 1.0	< 1.0	4.0
Cr	< 5.0	400.0	36.0	22.0	82.0
Ni	< 20.0	< 20.0	< 20.0	< 20.0	< 20.0
Co	4.0	33.0	48.0	36.0	56.0
Sc	18.0	19.0	40.0	22.0	29.0
Cu	31.0	29.0	36.0	71.0	36.0
Pb	5.0	0.5	3.0	5.0	24.0
Zn	< 50.0	77.0	130.0	140.0	491.0
Mo	< 1.0	< 1.0	< 1.0	3.0	< 1.0
W	2.0	< 1.0	3.0	< 1.0	17.0
As	2.0	16.0	8.3	2.3	3.7
Sb	0.3	0.6	< 0.1	0.7	0.7
Au	11	6	13	3	177
La	21.00	5.90	6.60	2.10	37.00
Ce	41.00	12.00	10.00	< 3.00	45.00
Nd	21.00	11.00	8.00	< 5.00	29.00
Sm	4.30	1.40	1.60	1.00	6.30
Eu	1.20	0.60	0.90	0.60	2.30
Tb	< 0.50	< 0.50	< 0.50	< 0.50	1.50
Yb	3.00	0.60	1.00	0.60	6.80
Lu	0.45	0.10	0.15	0.10	1.04

volatile contents (LOI) are raised considerably, which could be attributed to the influx of the externally derived mineralizing fluid (Klein, 1998) that have caused hydration (chloritization) and carbonatization reactions, in addition to the sulphidation of the host rock.

The trace elements (LILE and HFSE) display moderate to low contents, with positive anomalies of Ba and Sm, and a slightly negative anomaly of Zr (Fig. 5(a)), as well as depletion in Rb (Table 1). The Zr/Y (3.4–3.8), Rb/Sr (<0.07), Rb/Ba (<0.04), and K/Rb (>623) ratios are low, while the Ba/La (>17.6) ratio is moderate. This behavior is similar in both hydrothermally altered and least altered samples, except by the K enrichment shown by the altered microtonalite, which may be attributed to its retention by secondary sericite. The Rb depletion may be ascribed to the complete breakdown of the alkali feldspar and biotite (Pearce et al., 1984), and to the influence of aqueous hydrothermal fluids (Taylor et al., 1991). The REE show enriched and fractionated pattern of the LREE, a virtual absence of Eu anomaly and rather high contents of HREE (Fig. 5(b)). Comparing these chemical characteristics with those from tonalites and granodiorites of the Tromaí Suite (Fig. 5(a) and (b)), the HFSE and LILE patterns are similar, while the Caxias Microtonalite is a little more enriched in REE, especially in HREE, than the Tromaí granitoids. Nevertheless, both patterns are compatible with those of calc-alkaline, metaluminous, subduction-related granitoids found in Phanerozoic volcanic arcs, resembling either volcanic arc or post-collisional granitoids (Fig. 5(a) and (b)).

The schists exhibit low SiO_2 and alkali, and high iron contents, without significant differences between the two petrographic groups (biotite–chlorite-rich and quartz–sericite-rich). However, a distinction can be envisaged

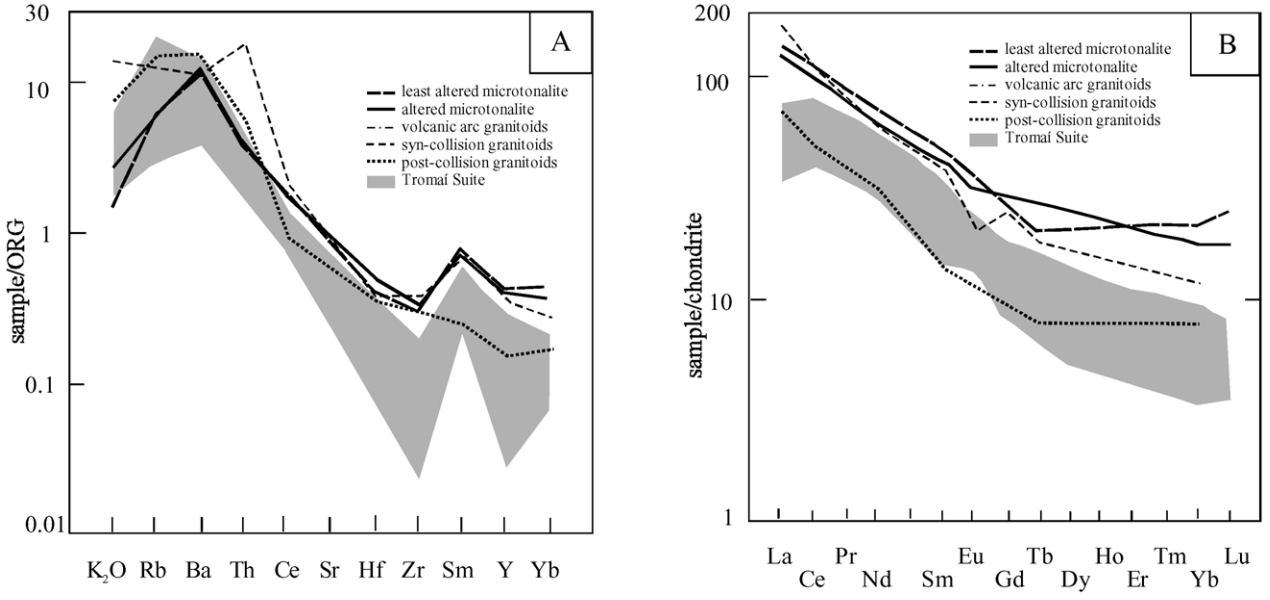

Fig. 5. (a) Spidergram and (b) REE patterns of the Caxias Microtonalite. Patterns of the Tromaí Suite and from modern orogenic granitoids are also displayed, for comparison.

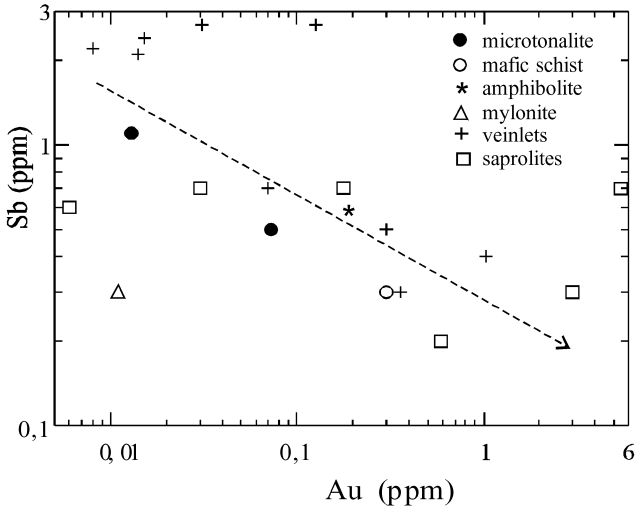

Fig. 6. Scattergram showing the negative correlation between Au and Sb in the Caxias gold deposit.

through the trace elements, as the biotite–chlorite schists show higher V, Co, Ni, Cr, and much lower Zr contents than the quartz–sericite schists (Table 1). These chemical and petrographic differences, as well as the presence of enclaves with the paragenesis amphibole + plagioclase + epidote + carbonate, are interpreted as product of the metamorphism of alternate layers of mafic volcanics and pelitic sediments, respectively, (a volcano-sedimentary sequence). A comparison of the chemical data with classical examples (e.g. Taylor and McLennan, 1985; Abouchami et al., 1990; Oberthür et al., 1994) supports this hypothesis.

The trace element composition of veins and veinlets crosscutting the schists and the microtonalite (Table 2), together with the petrographic characteristics and chemical signatures of the schists and microtonalite (Table 1), place some constraints on the geochemistry of the hydrothermal fluid. Elements such as As and Sb, which are commonly enriched in lode gold deposits, show generally low values at Caxias. Moreover, although subtle, Sb shows a negative correlation with gold (Fig. 6). Nickel, Co, V, and Cr, although reflecting the mafic provenance of part of the schists, are associated with higher concentrations of Au and As, reflecting the mineralization as well.

Introduction of H_2O, CO_2, K_2O, and S is suggested by the alteration assemblage (chlorite, carbonate, sericite, sulphides) as well as by the presence of CO_2-rich fluid inclusions in quartz (Klein, 1998; Klein et al., 2000b), and the chemical data show that the mineralization is characterized by low base metal contents. These features are typical of granitoid and greenstone hosted lode-gold mineralizations (Groves and Foster, 1991; Cassidy and Bennett, 1993).

Chemical analyses of saprolites from schists and the microtonalite (Table 3) have shown a similar pattern of element distribution, but Ba and Rb concentrations were observed to be greater in the saprolites than in the protoliths.

5. Geochronology

Geochronological analyses were performed at the Laboratório de Geologia Isotópica of the Universidade Federal do Pará (Pará-Iso), in order to determine the crystallization and crustal residence ages of the Caxias Microtonalite, employing the Pb evaporation technique in zircons and the Sm–Nd systematics, respectively.

5.1. Analytical procedures

Zircons for Pb evaporation analysis (Kober, 1986, 1987) were obtained after crushing and sieving the least altered microtonalite. Zircons were separated from the powdered material using magnetic and heavy liquid methods. Isotope analyses were performed on a Finnigan MAT 262 thermoionization mass spectrometer (TIMS), using the stepwise heating process. Data were acquired dynamically using the ion counting system of the instrument. The intensity of different Pb isotopes were measured in the mass sequence 206, 207, 208, 206, 207, 204, along 10 mass scans, defining one block of data with 18 $^{207}Pb/^{206}Pb$ ratios. Discrepant isotopic values were discarded using Dixon's test. Common Pb corrections were made according to Stacey and Kramers (1975) two-stage model, and only blocks with $^{206}Pb/^{204}Pb$ ratios higher than 2500 were used for apparent ages determinations.

Samples from the least altered and from the hydrothermally altered microtonalite were selected for Sm–Nd whole-rock analysis. The separation of Sm and Nd was carried out in two steps. Initially, the REE were separated from other elements by cation exchange chromatography using the 50wx-8 Dowex resin. Then, Sm and Nd were separated from the REE by anion exchange chromatography using the AG1-x4 Dowex resin, eluted with HNO_3–methanol. A mixed $^{150}Nd/^{149}Sm$ spike was used. The isotope analyses were carried out on the Finnigan MAT 262 TIMS. The Nd data were normalized to a $^{146}Nd/^{144}Nd$ ratio of 0.7219. During the period of analysis a $^{143}Nd/^{144}Nd$ ratio of 0.511835 ± 11 was obtained for the LaJolla Nd standard. Sm and Nd concentration for BCR-01 was 6.59 and 28.54 ppm, respectively. The crustal residence ages were calculated using the values of Michard et al. (1985) for the depleted mantle.

5.2. Isotopic data results and discussion

Zircon is a mineral with a very resistant crystalline structure and tends to preserve the isotopic information since its crystallization, despite latter magmatic, metamorphic, or alteration processes (Kober, 1986). Behaving as a robust system in respect to Pb, it yields apparent $^{207}Pb/^{206}Pb$ ages that can be quite similar to conventional and SHRIMP zircon ages (Kober, 1986; Ansdell and Kyser, 1991; Kröner and Tegtmeyer, 1994; Söderlund, 1996). In any case, the Pb zircon evaporation ages yield the minimum crystallization age of the host rock or protolith.

Table 4
Isotopic composition of radiogenic Pb of zircons from the least altered sample (CX 47) of the Caxias Microtonalite

Zircon	Evaporation, T (°C)	Number of measured ratios	$^{206}Pb/^{204}Pb$	$^{207}Pb/^{206}Pb$	$^{207}Pb/^{206}Pb$[a]	Age (Ma)
1	1480[a]	82	> 20.000	0.1203 ± 8	0.1200 ± 6	1965 ± 5
	1550[a]	18	> 20.000	0.1201 ± 6	0.1201 ± 6	1958 ± 5
2	1480[a]	90	> 20.000	0.1212 ± 4	0.1211 ± 4	1972 ± 4
	1550	88	> 20.000	0.1218 ± 4	0.1216 ± 4	1980 ± 3
4	1480	84	> 20.000	0.1222 ± 4	0.1220 ± 6	1985 ± 4
	1550	90	> 20.000	0.1223 ± 4	0.1220 ± 2	1986 ± 3
5	1480	70	> 20.000	0.1223 ± 6	0.1223 ± 6	1991 ± 5

[a] Heating steps not used in the age calculation.

Few zircon crystals were found in the analyzed sample, and only four of them were considered suitable for Pb evaporation age determinations. These zircon crystals were limpid, transparent, colorless to pink, subhedral to euhedral, and showing no signs of metamict texture.

The analytical results (Table 4) show that the ages obtained in the two evaporation/heating steps of the zircon-1 are quite distinct from those obtained from the other three zircons, which show a more consistent group of ages averaging 1985 ± 4 Ma. This zircon-1 was thus eliminated from the age calculation, and the age of 1985 ± 4 Ma may be considered the minimum crystallization age of the Caxias Microtonalite.

The Sm–Nd isotopes (Table 5) yielded crustal residence ages (T_{DM}) of 2.17 Ga and 2.00 Ga for the least altered and the hydrothermally altered samples, respectively. The $\varepsilon Nd(T)$ calculated backward from the present to the time of crystallization of the microtonalite shows a slightly positive value (+0.74) for the least altered sample and a little higher value (+3.02) for the hydrothermally altered sample. Present day values for the epsilon parameter $\varepsilon Nd(0)$ are quite similar: −16.13 and −16.29 for the least altered and hydrothermally altered samples, respectively.

Despite the resistance of the Sm–Nd whole-rock system to resetting even by high-grade metamorphism (Dickin, 1995), and the low solubility of the REE in natural aqueous solutions, high fluid/rock ratio may cause mobilization of the REE and/or fractionation of the Sm/Nd ratio (Rosing, 1990). In such a situation, changes in Nd model ages and in the initial εNd values may occur (Rosing, 1990; Patchett, 1992, and their references). A slight diminution in the LREE content of the hydrothermally altered sample of the microtonalite can be observed in Fig. 5(b), although the patterns remain similar. Nevertheless, this seems to have not affected greatly the isotopic results (Table 5), and the Nd data point to a juvenile origin for the protolith of the Caxias Microtonalite, and preclude any involvement of an Archean reworked component in its generation.

Similar T_{DM} model ages (2.12–2.19 Ga), with $\varepsilon Nd(T)$ ranging from +0.77 to +1.81, have been found for granitoids of the Rosário Suite (Moura and Gorayeb, unpublished data) (Table 6). Also, Sato (1998) reported a T_{DM} model age of 2.1 Ga for a granitoid of this same suite. The epsilon Nd parameter, recalculated from this data, is +2.47, also suggesting a juvenile source. Both these juvenile protoliths are less depleted than the normal depleted mantle at 2.1 Ga (εNd +5– + 6, according to DePaolo (1988)). A similar situation was reported by Doumbia et al. (1998) in the West African Craton. They related the source of the rocks to a less depleted mantle, such as a mantle plume, or to the involvement of a small amount of an older crust, which was not detected in the zircon studies that they have performed.

6. Discussion and concluding remarks

The Caxias gold deposit is hosted within a steeply dipping, NE-trending, oblique, transcurrent shear zone crosscutting schists from the Aurizona Group and the Caxias Microtonalite. Structural and petrographic evidence have shown that the hosting structure has had a protracted deformational history, ranging from early ductile to late brittle character. This evidence, together with previous fluid inclusion information, indicates that gold deposition occurred rather late in the shear zone development, under ductile–brittle conditions.

The hosting schists have been petrographically and chemically characterized as being derived from alternating sediments and mafic volcanic rocks, which have been transformed by metamorphism, respectively, to quartz–sericite

Table 5
Whole-rock Sm and Nd isotopic compositions and calculated model ages and εNd of the Caxias Microtonalite. CX 47: least altered sample; CX 65: hydrothermally altered sample

Sample	Sm (ppm)	Nd (ppm)	$^{147}Sm/^{144}Nd$	Error ($\times 10^{-5}$)	$^{143}Nd/^{144}Nd$	Error ($\times 10^{-5}$)	T_{DM} (Ga)	$\varepsilon Nd(T)$	$\varepsilon Nd(0)$
CX 47	9.03	41.67	0.13102	12	0.511811	5	2.17	+ 0.74	− 16.13
CX 65	6.60	32.80	0.12245	11	0.511803	7	2.00	+ 3.02	− 16.29

Table 6
Summary of the main geochronological data from granitoids of the São Luís Craton. WR: whole rock. References: (1) this study; (2) Costa et al. (1977); (3) Souza (1995); (4) Klein (unpublished data); (5) Gaudette et al. (1996); (6) Gorayeb et al. (1999); (7) Sato (1998); (8) Moura and Gorayeb (unpublished data)

Stratigraphic unit	Rock type	Method	Analysed material	Age (Ma)	Reference
Caxias Microtonalite	Microtonalite	Pb-evaporation	Zircon	1985 ± 4	Abouchami et al., 1990
		Sm–Nd	WR	2170 (T_{DM}); $\varepsilon Nd(T) = +0.74$	Abouchami et al., 1990
Tromaí Suite	Tonalite, trondhjemite	Rb–Sr	WR	2076 ± 96	Abreu, 1990
	Granitoid	Pb-evaporation	Zircon	2132 ± 18	Abreu et al., 1980
	Granodiorites/ tonalites/ trondhjemites	Pb-evaporation	Zircon	2148–2163	Almaraz and Cordani, 1969
Rosário Suite	Metagranitoids	Pb-evaporation	Zircon	2075–2146	Almeida, 2000; Almeida et al., 1968
	Metagranitoid	Sm–Nd	WR	2100 (T_{DM}); $\varepsilon Nd(T) = +2.47$[a]	Ansdell and Kyser, 1991
	Metagranitoids	Sm–Nd	WR	2120–2190 (T_{DM}); $\varepsilon Nd(T) =$ +0.77/ + 1.81	Bullard et al., 1965

[a] Recalculated from Sato (1998).

schists and chlorite–biotite schists. The latter have typically high V, Co, Ni, and Cr contents and low Zr contents.

The host rock association, structural setting, hydrothermal assemblage, and fluid properties and composition are similar to those of late-orogenic, structurally controlled gold deposits occurring in cratonic areas and metamorphic belts elsewhere in the world (e.g. Kerrich and Cassidy, 1994; Groves et al., 1998; Witt and Vanderhor, 1998).

6.1. The role of the Caxias Microtonalite

The spatial, and frequently temporal, association between syn- to late-tectonic small intrusions and lode-gold mineralization has been described in late-Archean cratons from Canada (Colvine et al., 1988), Zimbabwe (Vinyu et al., 1996) and Australia (Perring et al., 1991; Wang et al., 1993), but is uncommon in the Paleoproterozoic. These intrusions enclose late-magmatic, either porphyritic or equigranular felsic to intermediate rocks, in addition to silica-undersaturated rocks, occurring between 10 and 40 Ma after the end of the calc-alkaline volcanism in the greenstone belts. These rocks are largely undeformed, but tend to occur in deformation zones, sometimes in the same structures that host gold deposits. Also, narrow, gold-hosting, brittle–ductile shear zones often crosscut them.

Despite the clear spatial, and sometimes temporal, association between these intrusions and gold deposits, their genetic link is still controversial. Colvine et al. (1988) discarded the genetic relationship, based on the timing of the gold mineralizing event, which was considered late in relation to the emplacement of the plutons. Perring et al. (1991) also discarded a genetic link, envisioning the association, like Powell et al. (1991), as the expression of a deep tectonic–magmatic event, in which magmatism and mineralization utilize the same major structures for their emplacement. On the other hand, Wang et al. (1993) suggested a genetic link, at least in a provincial scale, and attributed to the granitoids, or to their sources, for the origin of the lead present in the mineralizing fluids.

In respect to the Caxias Microtonalite and the gold mineralization that it hosts, there is more evidence indicating the lack of a genetic relationship between them. First, the structural evidence suggests that gold had been introduced late in the structural development of the hosting shear zone. Second, the mineralizing fluid was defined as an externally derived, probably metamorphic, fluid (Klein, 1998; Klein et al., 2000b). Thus, the role of the microtonalite is interpreted as passive, in the sense that it did not contribute fluids to the mineralizing episode, but it might have contributed elements to the ore fluid at the site of gold deposition, through fluid-rock reactions. Moreover, its composition (Fe-rich) probably favored the breakdown of the gold-transporting complexes by reducing the sulphur activity of the fluid via pyrite precipitation, which is a very effective process for gold deposition. However, more isotopic data (Pb, S) are necessary to further assess the role of the microtonalite as a potential metal reservoir.

Also debatable is the relationship between the Caxias Microtonalite and the Tromaí Suite, which is the dominant lithology in the studied region. Chemically it is characterized by high Fe_2O_3 and low K_2O contents and by a metaluminous character. The patterns of REE and incompatible elements show some similarities with the Tromaí Suite. However, geochronological data suggest that the crystallization of the Caxias Microtonalite have occurred 100–150 Ma after the intrusion of the Tromaí Suite and the correlative Rosário Suite (Table 6), despite the coincident Sm–Nd model ages presented by the Caxias and Rosário units. Thus, the Caxias Microtonalite may represent either a very late manifestation of the Tromaí magmatism, or a juvenile, magmatic episode not described in the region yet, which may or may not be associated with the volcanism of the Aurizona metavolcanosedimentary sequence, occurring late in the magmatic–metamorphic–deformational event in which the gold-hosting sequences of the São Luís Craton were generated. Precise

U–Pb zircon studies are needed to evaluate further this hypothesis.

6.2. Implications for exploration

Rocks in the Gurupi region are strongly weathered. In such a situation, the geochemistry of the supergene alteration plays an important role in prospecting for ores and even in the mapping of concealed lithologies. The lateritization processes promote redistribution and chemical differentiation of gold and other elements in the weathering profile, in such a way that is of fundamental importance the recognition of which level of the profile is being sampled (Costa, 1993). According to this conception, even low values or concentrations lower than the background of the chemical elements may have geochemical significance. In addition, the accumulation of minerals that are more resistant to the weathering and the retention of chemical elements by clay minerals may cause considerable enrichments of some elements (Costa et al., 1991).

In the studied area the lateritic profiles are truncated at the saprolite level, with structures and mineralogy of the parent rocks partially visible and preserved. At this level, according to Costa (1993), the gold concentrations are quite similar to those of the protoliths.

In addition to gold, As, Sb, Ba, and Rb have shown to be the most prospective elements, as well as V, Cr, Co, and Ni, which not only indicate the mafic provenance of some schists, but also show enrichment consistent with the mineralization. These observations suggest that those elements may be useful indicators of mineralization, and thus might also be useful in the exploration for other mineral deposits in the region.

Acknowledgements

This paper holds part of E.L. Klein's MSc dissertation at Universidade Federal do Rio Grande do Sul (UFRGS). CNPq (National Research Council of Brazil) is acknowledged for providing a scholarship to E.L. Klein, and CPRM (Geological Survey of Brazil) is thanked for providing funds for the field and geochronological works. Valter Gama Avelar (UFPA) is thanked for analytical support, and Marcelo Lacerda Vasquez (CPRM) and Carlos Eduardo 'Cadu' de Mesquita Barros (UFPA) are acknowledged for comments on an early version of the manuscript. We are grateful to the journal reviewers, Drs Colombo C.G. Tassinari and Allen H. Fetter, whose thoughtful comments greatly improved this work.

References

Abouchami, W., Boher, M., Michard, A., Albarede, F., 1990. A major 2.1 Ga event of mafic magmatism in West Africa: an early stage of crustal accretion. Journal of Geophysical Research 95 (B11), 17605–17629.

Abreu, F.A.M., 1990. Evolução geotectônica do Pré-Cambriano da região Meio Norte do Brasil e sua correlação com a África Ocidental. Unpublished PhD thesis. Universidade Federal do Pará, Brazil, p. 440.

Abreu, F.A.M., Villas, R.N.N., Hasui, Y., 1980. Esboço estratigráfico do Precambriano da região do Gurupi, Estados do Pará e Maranhão. Boletim de Resumos Expandidos, XXXI Congresso Brasileiro de Geologia, Camboriú 2, 647–658.

Almaraz, J.S.U., Cordani, U.G., 1969. Delimitação entre as Províncias Geocronológicas Pré-Cambrianas ao longo do Rio Gurupi. Resumo das Conferências e Comunicações, XXIII Congresso Brasileiro de Geologia, Salvador (Boletim Especial, 1).

Almeida, H.G.G., 2000. Programa Levantamentos Geológicos Básicos do Brasil. Programa Grande Carajás. São Luís, folhas SA.23, escala 1:1.000.000. Estados do Pará e Maranhão. CPRM—Geological Survey of Brazil (on CD-ROM).

Almeida, F.F.M., Melcher, G.C., Cordani, U.G., Kawashita, K., Vandoros, P., 1968. Radiometric age determinations from northern Brazil. Boletim da Sociedade Brasileira de Geologia 17, 3–14.

Ansdell, K.M., Kyser, T.K., 1991. Plutonism, deformation, and metamorphism in the Proterozoic Flin Flon greenstone belt, Canada: limits on timing provided by the single-zircon Pb-evaporation technique. Geology 19, 518–521.

Bullard, E., Everett, J.E., Smith, A.G., 1965. The fit of the continents around the Atlantic. Symposium on continental drift. Philosophical Transactions of the Royal Society of London 258, 41–51.

Cassidy, K.F., Bennett, J.M., 1993. Gold mineralisation at the Lady Bountiful Mine, Western Australia: an example of a granitoid hosted Archaean lode gold deposit. Mineralium Deposita 28, 388–408.

Colvine, A.C., Fyon, J.A., Heather, K.B., Marmont, S., Smith, P.M., Troop, D.G., 1988. Archean lode gold deposits in Ontario. Ontario Geological Survey Miscellaneous Paper 139, p. 136.

Condie, K.C., 1982. Plate Tectonics and Crustal Evolution. Pergamon Press, New York.

Cordani, U.G., Melcher, G.C., Almeida, F.F.M., 1968. Outline of the Precambrian geochronology of South America. Canadian Journal of Earth Sciences 5, 629–632.

Costa, M.L., 1993. Gold distribution in lateritic profiles in South America, Africa, and Australia: applications to geochemical exploration in tropical regions. Journal of Geochemical Exploration 47, 143–163.

Costa, J.L., 2000. Programa Levantamentos Geológicos Básicos do Brasil. Programa Grande Carajás. Castanhal, Folha SA.23-V-C. Estado do Pará. CPRM—Geological Survey of Brazil, Belém, (on CD-ROM).

Costa, J.L., Ricci, P.S.F., 1995. A Faixa de Cisalhamento Gurupi e o cenário colisional do Cráton São Luís. Boletim de Resumos, V Simpósio Nacional de Estudos Tectônicos, Gramado, RS, pp. 18–20.

Costa, J.L., Araujo, A.A.F., Villas Boas, J.M., Faria, C.A.S., Silva Neto, C.S., Wanderley, V.J.R., 1977. Projeto Gurupi. Unpublished report. DNPM/CPRM, p. 258.

Costa, M.L., Angélica, R.S., Araújo, E.S., Horbe, A.M.C., 1991. Abundância e fracionamento dos elementos terras raras em lateritos maturos (crostas ferro-aluminosas e aluminosas) da Amazônia. Resumos, III Congresso Brasileiro de Geoquímica, São Paulo 2, 651–653.

DePaolo, D.J., 1988. Neodymium Isotope Geochemistry. An Introduction. Springer, Berlin.

Dickin, A.P., 1995. Radiogenic Isotope Geology. Cambridge University Press, Cambridge.

Doumbia, S., Pouclet, A., Kouamelan, A., Pecaut, J.J., Vidal, M., Delor, C., 1998. Petrogenesis of juvenile-type Birimian (Paleoproterozoic) granitoids in Central Côte-d'Ivoire West Africa: geochemistry and geochronology. Precambrian Research 87, 33–63.

Gaudette, H.E., Moura, C.A.V., Abreu, F.A.M., Gorayeb, P.S.S., 1996. Dados geocronológicos Pb–Pb em zircão de granitóides da Suíte Rosário. Anals, XXXIX Congresso Brasileiro de Geologia, Salvador 6, 508–511.

Gebre-Mariam, M., Hagemann, S.G., Groves, D.I., 1995. A classification scheme for epigenetic Archaean lode-gold deposits. Mineralium Deposita 30, 408–410.

Goodwin, A.M., 1996. Principles of Precambrian Geology. Academic Press, London.

Gorayeb, P.S.S., Gaudette, H.E., Moura, C.A.V., Abreu, F.A.M., 1999. Geologia e geocronologia da Suíte Rosário, nordeste do Brasil, e sua contextualização geotectônica. Revista Brasileira de Geociências 29 571–578.

Groves, D.I., Foster, R.P., 1991. Archean lode gold deposits. In: Foster, R.P. (Ed.). Gold Metallogeny and Exploration. Blackie and Son, Glasgow, pp. 63–103.

Groves, D.I., Goldfarb, R.J., Gebre-Mariam, M., Hagemann, S., Robert, F., 1998. Orogenic gold deposits: a proposed classification in the context of their crustal distribution and relationship to other gold deposits types. Ore Geology Reviews 13, 7–27.

Hurley, P.M., Almeida, F.F.M., Melcher, G.C., Cordani, U.G., Rand, J.R., Kawashita, K., Vandoros, P., Pinson, W.H., Fairbairn, H.W., 1967. Test of continental drift by comparison of radiometric ages. Science 157, 495–500.

Kerrich, R., Cassidy, K.F., 1994. Temporal relationships of lode gold mineralization to accretion, magmatism, metamorphism and deformation-Archean to present—a review. Ore Geology Reviews 9, 263–310.

Klein, E.L., 1998. Aspectos geoquímicos, geocronológicos e estudo dos fluidos associados às mineralizações auríferas dos garimpos Caxias e Areal, Cráton de São Luís, noroeste do Maranhão. Unpublished MSc dissertation. Universidade Federal do Rio Grande do Sul, Brazil, p. 189.

Klein, E.L., Koppe, J.C., 2000. Chlorite geothermometry and physicochemical conditions of gold mineralization in the Paleoproterozoic Caxias deposit São Luís Craton, northern Brazil. Geochimica Brasiliensis 14 (1).

Klein, E.L., Fuzikawa, K., Dantas, M.S.S., 2000a. Fluids associated to the Paleoproterozoic Pedra de Fogo gold mineralisation, São Luís Craton, Brazil. Abstracts volume, XXXI International Geological Congress, Rio de Janeiro (on CD-ROM).

Klein, E.L., Fuzikawa, K., Koppe, J.C., 2000b. Fluid inclusion studies on Caxias and Areal gold mineralizations São Luís Craton, northern Brazil. Journal of Geochemical Exploration 71, 51–72.

Kober, B., 1986. Whole-grain evaporation for $^{207}Pb/^{206}Pb$-age-investigations on single zircons using a double-filament source. Contributions to Mineralogy and Petrology 93, 482–490.

Kober, B., 1987. Single grain evaporation combined with Pb + emitter bedding for $^{207}Pb/^{206}Pb$ investigations using thermal ion mass spectrometry, and implications for zirconology. Contributions to Mineralogy and Petrology 96, 63–71.

Kröner, A., Tegtmeyer, A., 1994. Gneiss–greenstone relationships in the Ancient Gneiss Complex of southwestern Swaziland, southern Africa, and implications for early crustal evolution. Precambrian Research 67, 109–139.

Leão Neto, R., 1993. Projeto Carutapera; Baixada Maranhense, informe anual de projeto, 1992. CPRM/DEPEM. Unpublished report.

Ledru, P., Johan, V., Milési, J.P., Tegyey, M., 1994. Markers of the last stages of the Palaeoproterozoic collision: evidence for a 2 Ga continent involving circum-South Atlantic provinces. Precambrian Research 69, 169–191.

Lesquer, A., Beltrão, J.F., Abreu, F.A.M., 1984. Proterozoic links between northeastern Brazil and West Africa: a plate tectonic model based on gravity data. Tectonophysics 110, 9–26.

Michard, A., Gurriet, P., Soudant, M., Albarede, F., 1985. Nd isotopes in French phanerozoic shales: external vs internal aspects of crustal evolution. Geochimica et Cosmochimica Acta 49, 601–610.

Oberthür, T., Vetter, U., Schmidt Mumm, A., Weiser, T., Amanor, J., Gyapong, W.A., Kumi, R., Blenkinsop, T.G., 1994. The Ashanti gold mine at Obuasi in Ghana: mineralogical, geochemical, stable isotope and fluid inclusion studies on the metallogenesis of the deposit. Geologische Jahrbuch D100, 31–129.

Park, R.G., 1989. Foundations of Structural Geology. Blackie and Son, Glasgow.

Pastana, J.M.N., 1995. Programa Levantamentos Geológicos Básicos do Brasil. Programa Grande Carajás. Turiaçu/Pinheiro, folhas SA.23-V-D/SA.23-Y-B. Estados do Pará e Maranhão. CPRM—Geological Survey of Brazil, p. 205.

Patchett, P.J., 1992. Isotopic studies of Proterozoic crustal growth and evolution. In: Condie, K.C. (Ed.). Proterozoic Crustal Evolution. Elsevier, Amsterdam, pp. 481–508.

Pearce, J.A., Harris, N.B.W., Tindle, A.G., 1984. Trace elements discrimination diagrams for the tectonic interpretation of granitic rocks. Journal of Petrology 25, 956–983.

Perring, C.S., Groves, D.I., Shellabear, J.N., Hallberg, J., 1991. The 'porphyry-gold' association in the Norseman–Wiluna Belt of Western Australia: implications for models of Archaean gold metallogeny. Precambrian Research 51, 85–113.

Powell, R., Will, T.M., Phillips, G.N., 1991. Metamorphism in Archaean greenstone belts: calculated fluid compositions and implication for gold mineralization. Journal of Metamorphic Geology 9, 141–150.

Ramsey, J.G., Huber, M.I., 1987. The Techniques of Modern Structural Geology. Academic Press, New York.

Rodrigues, T.L.N., Araújo, C.C., Camozzato, E., Ramgrab, G.E., 1994. Programa Levantamentos Geológicos Básicos. São Luís, Folha SA.23-Z-A. Cururupu, Folha SA.23-X-C. Estado do Maranhão—Escala 1:250.000. CPRM—Geological Survey of Brazil, Brasília, p. 185.

Rosing, M.T., 1990. The theoretical effect of metasomatism on Sm–Nd isotopic systems. Geochimica et Cosmochimica Acta 54, 1337–1341.

Sato, K., 1998. Evolução crustal da Plataforma Sul Americana com base na geoquímica Sm–Nd. Doctoral thesis, Universidade de São Paulo, Brazil, p. 301.

Smith, T.E., 1992. Volcanic rocks of early Proterozoic greenstone belts. In: Condie, K.C. (Ed.). Proterozoic Crustal Evolution. Elsevier, Amsterdam, pp. 7–54.

Söderlund, U., 1996. Conventional U–Pb dating versus single-zircon Pb evaporation dating of complex zircons from a pegmatite in the high-grade gneisses of southwestern Sweden. Lithos 38, 93–105.

Souza, D.J.L., 1995. Estudo geocronológico das rochas tonalíticas de Igarapé de Areia-Nordeste do Pará. Resumos, Seminário de Iniciação Científica. Universidade Federal do Pará, Brazil (Unpubulished).

Stacey, J.S., Kramers, J.D., 1975. Approximation of terrestrial lead isotope evolution by a two-stage model. Earth and Planetary Sciences Letters 26, 207–221.

Taylor, S.R., McLennan, S.M., 1985. The continental crust: its composition and evolution. An examination of the geochemical record preserved in sedimentary rocks. , Geoscience Texts. Blackwell Scientific Publications, Oxford.

Taylor, P.N., Kramers, J.D., Moorbath, S., Wilson, J.F., Orpen, J.L., Martin, A., 1991. Pb/Pb, Sm–Nd and Rb–Sr geochronology in the Archean Craton of Zimbabwe. Chemical Geology (Isotope Geology Section) 87, 175–196.

Vinyu, M.L., Frei, R., Jelsma, H.A., 1996. Timing between granitoid emplacement and associated gold mineralization: examples from the ca. 2.7 Ga Harare–Shamva greenstone belt, northern Zimbabwe. Canadian Journal of Earth Sciences 33, 981–992.

Wang, L.G., McNaughton, N.J., Groves, D.I., 1993. An overview of the relationship between granitoid intrusions and gold mineralisation in the Archaean Murchinson Province, Western Australia. Mineralium Deposita 28, 482–494.

Witt, W.K., Vanderhor, F., 1998. Diversity within a unified model for Archaean gold mineralization in the Yilgarn Craton of Western Australia: an overview of the late-orogenic, structurally-controlled gold deposits. Ore Geology Reviews 13, 29–64.

Yamaguti, H.S., Villas, R.N.N., 1999. A mineralização aurífera de Montes Áureos (NW do Maranhão): aspectos geológicos e fluidos mineralizantes. Boletim de resumos, VI Simpósio de Geologia da Amazônia, Manaus, AM, pp. 102–105.